구조 비선형성 및 충격파 간섭효과를 고려한 미사일 날개의 천음속 유체유발 진동특성

Characteristics of Transonic Flow-Induced Vibration for a Missile Wing Considering Structural Nonlinearity and Shock Inference Effects

김동현*·이 인**·김승호***·김태연¥·James S. Lee¥

Dong-Hyun Kim*, In Lee, Seung-Ho Kim***, Taehyoun Kim¥, and James S. Lee¥**

Key Words : Flow-induced vibration, Fluid-Structure interaction, Navier-Stokes, CFD, CSD, MAV, Nonlinear vibration, Flow separation, SIMPLE, SIP, CTIM

ABSTRACT

Nonlinear flow-induced vibration characteristics of a generic missile wing (or control surface) are investigated in this study. The wing model has freeplay structural nonlinearity at its pitch axis. Nonlinear aerodynamic flows with unsteady shock waves are considered in the transonic flow region. To practically consider the effects of freeplay structural nonlinearity, the fictitious mass method (FMM) is applied to structural vibration analysis based on a finite element method (FEM). A computational fluid dynamics (CFD) technique is used for computing the nonlinear unsteady aerodynamics of all-movable wings. The aerodynamic analysis is based on the efficient transonic small-disturbance aerodynamic equations of motion using the potential-flow theory. To solve the nonlinear aeroelastic governing equations including the freeplay effect, a modal-based computational structural dynamic (CSD) analysis technique based on fictitious mass method (FMM) is used in time-domain. In addition, CSD and unsteady CFD techniques are simultaneously coupled to give accurate computational results. Various aeroelastic computations have been performed for a generic missile wing model. Linear and nonlinear aeroelastic computations have been conducted and the characteristics of flow-induced vibration are introduced.

1. Introduction

Flutter (typical flow-induced vibration of high-speed aero-vehicle wings) calculations are generally performed with the assumption of a linear aerodynamic and linear structural model. However, there are two typical nonlinearities in general high-speed aeroelastic problems. One is aerodynamic nonlinearity and the other is structural nonlinearity. Aerodynamic nonlinearities can be attributed to shock waves, separated turbulence flow, vortex interaction, etc. Structural nonlinearities are subdivided into distributed nonlinearities and concentrated ones. Distributed nonlinearities are spread over the entire structure like material and geometric nonlinearities. However, concentrated nonlinearities have local effects in a control mechanism or an attachment of external stores. The concentrated structural nonlinearities typically include freeplay, friction, bilinear spring, hysteresis, and preload. Concentrated structural nonlinearities can be normally generated from worn and loose phenomena of control surface connections, manufacturing tolerances, etc. Among all these several nonlinearities, the freeplay tends to give the most critical aeroelastic instabilities. In addition, during the service life of a flight vehicle, the level of freeplay will normally increase due to wear of bearings. Thus, most flight vehicles may inherently have this kind of concentrated structural nonlinearities. To date, there have been a few predominant studies on aeroelastic problems of three-dimensional wings with concentrated structural nonlinearities.[1-4] Even though, computational studies including both the structural nonlinearity and the aerodynamic nonlinearity related to shock waves can hardly be found.

The influence of the freeplay on the wing flutter characteristics can be also emphasized in the transonic and supersonic flow regions with shock waves. In addition, development of an accurate and effective computation technique is important in a design process. The focus of this paper is to show the freeplay effects on nonlinear aeroelastic characteristics of an all-movable wing with shock wave interferences. Because of the sweptback planform shape, both the bending and torsion frequencies and mode shapes are affected by the pitch actuator stiffness. To effectively consider the effects of freeplay structural nonlinearity, a fictitious mass method (FMM)[5-6] is applied to structural vibration analysis based on finite element method (FEM). Nonlinear unsteady aerodynamics is also considered in transonic and supersonic flow regions. The TSD3KR code[7-9] based on the transonic small-disturbance equation was used to

* 경상대학교 기계항공공학부
E-mail: *dhk@nongae.gsnu.ac.kr*
Tel: (055) 751-6125, Fax: (055) 755-2081
** 한국과학기술원 기계공학과 (항공우주공학전공)
*** 한국항공우주산업㈜
¥ The Boeing Company (Seattle, WA)

efficiently compute the transonic and supersonic aerodynamics. Computational structural dynamic (CSD) analyses have been performed using a finite element method. For the solution of the nonlinear aeroelastic governing equations, a modal-based computational structural dynamic (CSD) analysis technique based on FMM is used in time-domain. It simultaneously coupled with unsteady CFD technique to give accurate simulation results. Nonlinear aeroelastic time responses are computed by this simultaneous coupled time-integration method (CTIM). Various aeroelastic computations have been performed and the results are presented and compared with a linear structural case. From the present study, it is typically shown that the effect of freeplay nonlinearity tends to strongly decrease the aeroelastic stability of an all-movable missile wing in high-speed flows with strong shock interferences.

2. Theoretical Background

2.1 Normal Mode Analysis Using FMM

In nonlinear aeroelastic problems with concentrated structural nonlinearities, structural properties are varying as the displacement changes. Hence, using a constant normal mode from a fixed structural model gives inaccurate results. To overcome this kind of problem, the fictitious mass method (FMM) proposed by Karpel[5-6] is applied in this study. Neglecting the effect of structural damping, free vibration (air off) equation of motion of an n degrees-of-freedom system with fictitious masses (FMs) can be given as

$$[M+M_f]\{\ddot{u}(t)\}+[K]\{u(t)\}=\{0\} \tag{1}$$

where the fictitious masses is added to the corresponding degrees-of-freedom where structural changes occur. This means that the elements of the fictitious mass matrix $[M_f]$ are zero, except for the terms added to the structure at the locations of subsequent large structural variations. From the normal mode analysis using a finite element method, the generalized mass and stiffness matrix are given as

$$[GM_f]=[\phi_f]^T[M+M_f][\phi_f] \tag{2}$$

$$[GK_f]=[\phi_f]^T[K][\phi_f]=[\omega_f^2][GM_f] \tag{3}$$

where $[\omega_f]$ is a diagonal matrix of the natural frequencies including zero frequencies for rigid-body modes. Here, the size of generalized matrices directly depends on the selected number of fictitious natural vibration mode for further analysis.

It is known that the fictitious mass modes can serve as a constant set of generalized coordinates for a wide range of structural variations in the vicinity of the applied fictitious masses. Thus, it can be assumed that the displacement vector {u} of an actual nonlinear system can be expressed as a linear combination of the fictitious mass modes as follows:

$$\{u\}=[\phi_f]\{q_f\} \tag{4}$$

Using above transformation equation, we can drive the following normalized eigenvalue problem

$$\begin{aligned}&[\phi_f]^T[M-M_f][\phi_f]\{\ddot{q}_f(t)\}\\&+[\phi_f]^T[K+\Delta K][\phi_f]\{q_f(t)\}=\{0\}\end{aligned} \tag{5}$$

or

$$\begin{aligned}&([GM_f]-[\phi_f]^T[M_f][\phi_f])\{\ddot{q}_f(t)\}\\&+([GK_f]+[\phi_f]^T[\Delta K][\phi_f])\{q_f(t)\}=\{0\}\end{aligned} \tag{6}$$

From above equations, we can obtain the natural frequencies, $[\omega_b]=[\omega_a]$, of the actual structure with local stiffness variations (without fictitious masses) and the base square eigenvector matrix, $[\chi_b]$. Since an all movable wing is considered in this study, the stiffness variations at the pitch (or spindle) axis is just considered. Here, the accuracy of the obtained natural frequencies tends to dominantly depend on the scale of $[M_f]$. Generally, a large positive value of $[M_f]$ is recommended unless arising numerical singularity problems in calculating the eigenvalue solution of Eq. (1). By conducting some trial and error computations, we can find an appropriate value of $[M_f]$ giving a converged solution. The fictitious masses need to facilitate wide ranges of stiffness variations have to be significantly larger than the corresponding nominal masses of attaching nodal points.

For computational convenience, let us define the following base modal matrix as

$$[\phi_b]=[\phi_f][\bar{\chi}_b] \tag{7}$$

where $[\bar{\chi}_b]$ is a mass normalized square eigenvector matrix of $[\chi_b]$ and satisfies the following relation.

$$[\bar{\chi}_b]^T([GM_f]-[\phi_f]^T[M_f][\phi_f])[\bar{\chi}_b]=[I] \tag{8}$$

2.2 Nonlinear Aeroelastic Modeling

The aeroelastic equations of motion for an elastic wing with concentrated structural nonlinearity is written as follows:

$$[M]\{\ddot{u}(t)\}+[C]\{\dot{u}(t)\}+[R(u)]=\{F(t,u,\dot{u})\} \tag{9}$$

where [K(u)] is nonlinear stiffness matrix which is a function of displacement. For piecewise nonlinearity, nonlinear stiffness matrix can be written as follows:

$$[R(u)]=[KL]\{u\}+\{f(\alpha)\} \tag{10}$$

where $[KL]$ is a linear stiffness matrix of the all movable wing without pitch freeplay stiffness, and $\{f(\alpha)\}$ is the nonlinear restoring force vector whose element are zero except for nonlinear element. For a freeplay nonlinearity, $\{f(\alpha)\}$ is given as follows:

$$f(\alpha)=\begin{cases} K_\alpha(\alpha-s), & \alpha > s \\ 0, & -s \le \alpha \le s \\ K_\alpha(\alpha+s), & \alpha < -s \end{cases} \tag{11}$$

where α is a pitch displacement and s is a magnitude of freeplay angle. Let's introduce the following transformation relation based on the FMM.

$$\{u(t)\}=[\phi_b]\{q(t)\} \tag{12}$$

Using Eq. (12), the governing aeroelastic equation of motion can be reformulated in terms of generalized displacement vector $\{q(t)\}$ which is a solution of the following equation:

$$[M_g]\{\ddot{q}(t)\}+[C_g]\{\dot{q}(t)\}+[R_g(q)]=\{Q(t,q,\dot{q})\} \tag{13}$$

where

$$[M_g]=[\phi_b]^T[M][\phi_b]$$
$$=[\overline{\chi}_b]^T([GM_f]-[\phi_f]^T[M_f][\phi_f])[\overline{\chi}_b]$$
$$[C_g]=[\phi_b]^T[C][\phi_b]=2[\zeta_b][\omega_b]$$
$$[R_g(q)]=[\phi_b]^T[KL][\phi_b]+[\phi_b]^T\{f(\alpha)\}$$
$$=[\chi_b]^T[GK_f][\chi_b]+[\phi_b]^T\{f(\alpha)\}$$
$$\{Q\}=[\tilde{\phi}_b(x,y)]^T\{\tilde{F}(x,y,t)\},\ [\tilde{\phi}_b]=[G_{kg}][\phi_b]$$

Here, $[G_{kg}]$ is a transformation matrix for surface spline of modal matrix from FEM node to CFD grid. {F} is the external force vector due to unsteady aerodynamic flows around a wing. It is computed on the CFD grids of the wing surface and can be obtained by integrating the instantaneous unsteady pressure distributions as

$$\overline{F}(x,y,t)=\frac{1}{2}\rho_\infty U_\infty^2 c_r^2 \iint_S (Cp_L(x,y,t)-Cp_U(x,y,t))\frac{dS}{c_r^2} \tag{14}$$

In Eq. (14), unsteady pressure coefficients, Cp, are directly computed from TSD aerodynamic analyses, which are simultaneously coupled with Eq. (13). Then, the unsteady aerodynamic forces for each cell area (Eq. (14)) are numerically integrated using a two-point Gaussian quadrature formula. In this study, to fully consider the characteristics of aeroelastic responses, the coupled-time integration method (CTIM) has been used.

Introducing the state vector {x} to perform the efficient numerical calculation, Eq. (3) can be written in the first order form as

$$\{\dot{x}(t)\}=[A]\{x(t)\}+[B]\{u(t)\} \tag{15}$$

where

$$[A]=\begin{bmatrix} [0] & [I] \\ -[M_g]^{-1}[\chi_b]^T[GK_f][\chi_b] & -[M_g]^{-1}[C_g] \end{bmatrix}$$
$$[B]=\begin{bmatrix} [0] \\ [M_g]^{-1} \end{bmatrix},\ \{u(t)\}=\begin{Bmatrix} \{0\} \\ \{Q(t)-[\phi_b]^T\{f(\alpha)\}\} \end{Bmatrix}$$
$$\{x(t)\}=\begin{Bmatrix} \{q(t)\} \\ \{\dot{q}(t)\} \end{Bmatrix}$$

Generally, to calculate the time response of Eq. (5) due to the initial condition, external forces or control inputs are needed to analyze the behavior of the system. For the nonlinear aeroelastic systems, the 5th order Runge-Kutta algorithm can be typically used for accuracy.

2.3 Time-Domain Unsteady Aerodynamics

Nonlinear Aerodynamic Theory

The modified transonic small disturbance (TSD) potential equation transformed into the computational domain can be written in the strong conservation form as

$$\begin{aligned} &-\frac{\partial}{\partial\tau}\left[\frac{M^2}{\xi_x}\phi_\tau+2M^2\phi_\xi\right] \\ &+\frac{\partial}{\partial\xi}\left[(1-M^2)\xi_x\phi_\xi-\frac{1}{2}(\gamma+1)M^2\xi_x^2\phi_\xi^2\right. \\ &+\frac{1}{2}(\gamma-3)M^2(\xi_y\phi_\xi+\phi_\eta)^2+\frac{\xi_y}{\xi_x}(\xi_y\phi_\xi+\phi_\eta) \\ &\left.-(\gamma-1)M^2\xi_y\phi_\xi(\xi_y\phi_\xi+\phi_\eta)\right] \\ &+\frac{\partial}{\partial\eta}\left[\frac{1}{\xi_x}(\xi_y\phi_\xi+\phi_\eta)-(\gamma-1)M^2\phi_\xi(\xi_y\phi_\xi+\phi_\eta)\right] \\ &+\frac{\partial}{\partial\varsigma}\left[\frac{1}{\xi_x}\phi_\varsigma\right]=0 \end{aligned} \tag{16}$$

where M is a freestream Mach number, ϕ is the small-disturbed potential and τ is the nondimensional time. Here, ϕ and τ are normalized as the reference chord length and freestream velocity, respectively. In Eq. (16), ξ, η, and ς represent the axes in the computational domain, which correspond to x-, y- and z-axes in the nondimensional physical coordinates of the streamwise, spanwise, and vertical directions, respectively. The small-disturbed potential, ϕ, is defined from the full potential Φ as

$$\Phi(\tilde{x},\tilde{y},\tilde{z},t)=U_\infty c_r[x+\phi(x,y,z,\tau)] \tag{17}$$

In this study, the physical dimensions $\tilde{x}, \tilde{y}, \tilde{z}$ and t are nondimensionalized as

$$x=\frac{\tilde{x}}{c_r},\quad y=\frac{\tilde{y}}{c_r},\quad z=\frac{\tilde{z}}{c_r},\quad \tau=\frac{tU_\infty}{c_r} \tag{18}$$

Equation (19) is solved using a time-accurate approximate factorization (AF) algorithm[12]. The AF algorithm consists of a time linearization procedure coupled with internal subiterations. After Eq. (16) is written at the advanced time level n+1, internal subiterations performed at each intermediate time (*) levels.

$$\left.\frac{\partial R}{\partial \phi}\right|^{*}\Delta\phi=-R(\phi^{*}) \tag{19}$$

where $\Delta\phi=\phi^{n+1}-\phi^{*}$ and if $\Delta\phi$ approaches to zero then ϕ^{*} is equal to ϕ^{n+1}. The left side of Eq. (19) is then be approximately factorized into the following three operators:

$$L_\xi L_\eta L_\zeta \Delta\phi=-R(\phi^{*},\phi^{n},\phi^{n-1},\phi^{n-2}) \tag{20}$$

where the operators are defined as

$$\begin{aligned}L_\xi=1&+\frac{3\Delta t}{2}\xi_x\frac{\partial}{\partial\xi}-\frac{\Delta t^2}{2}\frac{\partial}{\partial\xi}\left(\frac{1-M^2}{M^2}\xi_x^{\,2}\right.\\&-(\gamma+1)\xi_x^{\,3}\phi_\xi^{*}+(\gamma-3)\xi_x^{\,2}(\xi_y\phi_\xi^{*}+\phi_\eta^{*})\\&+\xi_y^{2}(1-(\gamma-1)\xi_x\phi_\xi^{*})\\&\left.-(\gamma-1)M^2\xi_y(\xi_y\phi_\xi^{*}+\phi_\eta^{*})\right)\frac{\partial}{\partial\xi}\end{aligned} \tag{21}$$

$$L_\eta=1-\frac{\Delta t^2}{2}\frac{\partial}{\partial\eta}\left(\frac{1-(\gamma-1)M^2}{M^2}\right)\frac{\partial}{\partial\eta} \tag{22}$$

$$L_\zeta=1-\frac{\Delta t^2}{2}\frac{\partial}{\partial\zeta}\left(\frac{1}{M^2}\right)\frac{\partial}{\partial\zeta} \tag{23}$$

$$\begin{aligned}R=&\frac{2\phi^{*}-5\phi^{n}+4\phi^{n-1}-\phi^{n-2}}{2}\\&+\xi_x\Delta t^2\left(\frac{3\phi_\xi^{*}-4\phi_\xi^{n}+\phi_\xi^{n-1}}{2}\right)\\&-\frac{\Delta t^2}{2}\left[\frac{\partial}{\partial\xi}\left\{\frac{1-M^2}{M^2}\xi_x^{\,2}\phi_\xi^{*}-\frac{(\gamma+1)}{2M^2}\xi_x^{3}\phi_\xi^{*2}\right.\right.\\&-\frac{(\gamma-3)}{2(\gamma+1)}\xi_x(\xi_y\phi_\xi^{*}+\phi_\eta^{*})^2\\&\left.+\frac{\xi_y}{M^4}(\xi_y\phi_\xi^{*}+\phi_\eta^{*})-\frac{(\gamma-1)}{M^2}\xi_x\xi_y\phi_\xi^{*}(\xi_y\phi_\xi^{*}+\phi_\eta^{*})\right\}\\&+\frac{\partial}{\partial\eta}\left\{\frac{1}{M^2}(\xi_y\phi_\xi^{*}+\phi_\eta^{*})-(\gamma-1)\xi_x\phi_\xi^{*}(\xi_y\phi_\xi^{*}+\phi_\eta^{*})\right\}\\&\left.+\frac{\partial}{\partial\zeta}\left\{\frac{1}{M^2}\phi_\zeta^{*}\right\}\right]\end{aligned} \tag{24}$$

Detailed theoretical background and validation of the present study for the clean wing and the wing with control surface can be found from Ref. 7. The aerodynamic analysis results for more advanced applications can also be found from Ref. 8.

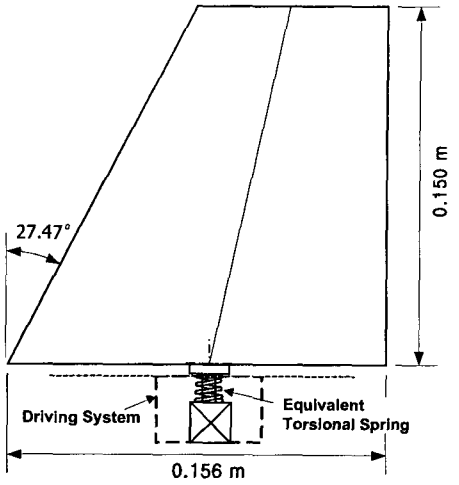

Fig. 1 Geometric configuration of a generic missile wing.

Table 1 Comparison of natural frequencies for the all-movable wing model

Mode	Direct Model		FM model
	K_α=120 Nm/rad	K_α=0 Nm/rad	K_α=120 Nm/rad
1	73.9 Hz	0.0 Hz	73.9 Hz
2	127.5 Hz	96.2 Hz	127.5 Hz
3	382.9 Hz	382.5 Hz	382.9 Hz
4	454.9 Hz	438.1 Hz	454.9 Hz
5	692.1 Hz	691.4 Hz	692.1 Hz
6	956.5 Hz	947.7 Hz	956.1 Hz

3. Results and Discussion

As a numerical example, a typical all-movable missile wing is considered for nonlinear aeroelastic simulations with the shock wave effects. Fig. 1 shows the general configuration of the present all-movable wing model. The aspect ratio of the wing is 2.564, taper ratio is 0.5, and swept-back angle of leading edge is 27.47 degree. The wing section is assumed as 5% biconvex airfoil. There is no aerodynamic twist but linear spanwise thickness variation. The root chord thickness and tip chord thickness are 3 mm and 1.5 mm, respectively. The material of wing is aluminum alloy and its properties are E=72.4 GPa, ν=0.33 and ρ_S=2713 kg/m^3. The structural model was built up from plate, rod, spring, and concentrated mass elements. The wing is connected by a spindle axis with a torsion spring. Natural vibration analyses are performed using MSC/NASTRAN (Ver.70.5). The plate, spring and fictitious mass are

modeled as CQUAD8, CMASS2 and CELAS2 elements, respectively. Natural mode shape vectors are mass normalized in this study. The wing is divided by 4×4 using eight node element (CQUAD8). It is experienced from this study that the use of DMAP module of MSC/NASTRAN is needed to increase the numerical accuracy.

The comparison of computed lowest eight natural frequencies are presented in Table 1. One can see that fictitious mass (FM) model can accurately predict the natural frequencies of the original wing structure. For this computation, a concentrated inertia of 50000 Nm^2 is imposed at the nodal point of spindle connection.

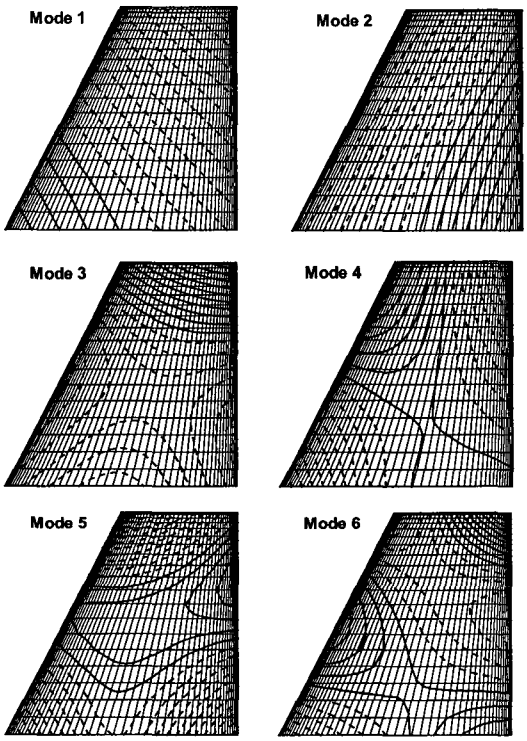

Fig. 2 Natural vibration mode shapes interpolated on CFD grid (K_α=120 Nm/rad).

Surface spline technique based on the infinite plate theory is used to interpolate natural mode shapes on the aerodynamic wing surface grid. Interpolated natural vibration mode shapes are also presented in Fig. 2. Here, the dashed lines mean the negative values of natural mode vectors.

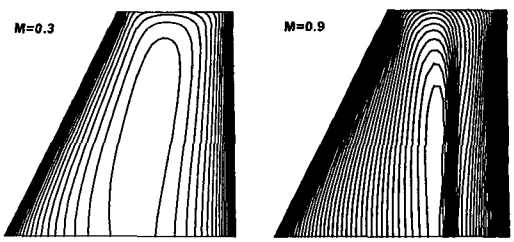

Fig. 3 Comparison of free vibration responses.

Figure 3 shows the steady pressure distribution of the missile wing at M=0.3 and M=0.9. Here, one can see the normal shock wave on the wing surface at M=0.9.

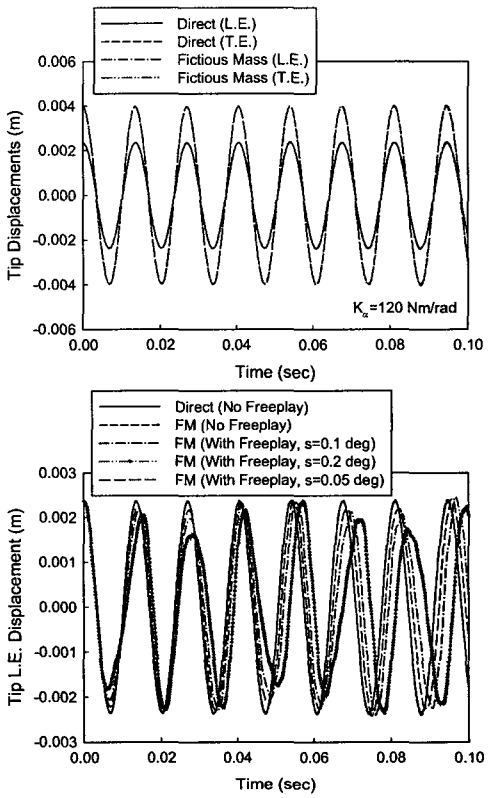

Fig. 4 Comparison of free vibration responses (linear and nonlinear cases).

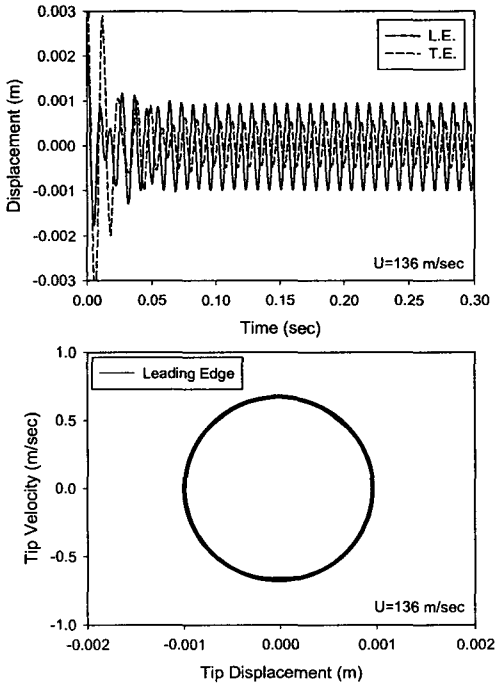

Fig. 5 Comparison of aeroelastic response for the linear model without freeplay (M=0.3, α_0=0 deg)

Figure 4 shows the free vibration responses at wing tip. Linear and nonlinear structural model are considered. To validate FM method, two-different approaches (direct vs. FM) are simultaneously compared and one can see very good agreement. Nonlinear responses for various freeplay angles are also presented to show the effect of freeplay. Here, it can be shown that increasing the freeplay angle, decreasing the frequency of a structural response. This physically means the reduction of equivalent stiffness.

Figure 5 shows neutral aeroelastic responses of a linear structure model at M=0.3. For this low speed Mach number no shock wave interference is expected. Several computations have been conducted to find these neutral responses. Its phase diagram also shows a typical linearity of ideal circle shape. Figure 6 shows several nonlinear aeroelastic responses in the transonic flow of Mach 0.9. One can see typical limit cycle oscillations (LCO) for several dynamic pressure conditions. In this case, the freeplay angle is assumed as 0.2 deg and generalized displacement of the first mode is imposed as an initial condition. This case contains two kinds of nonlinearities such as a freeplay and a transonic normal shock wave.

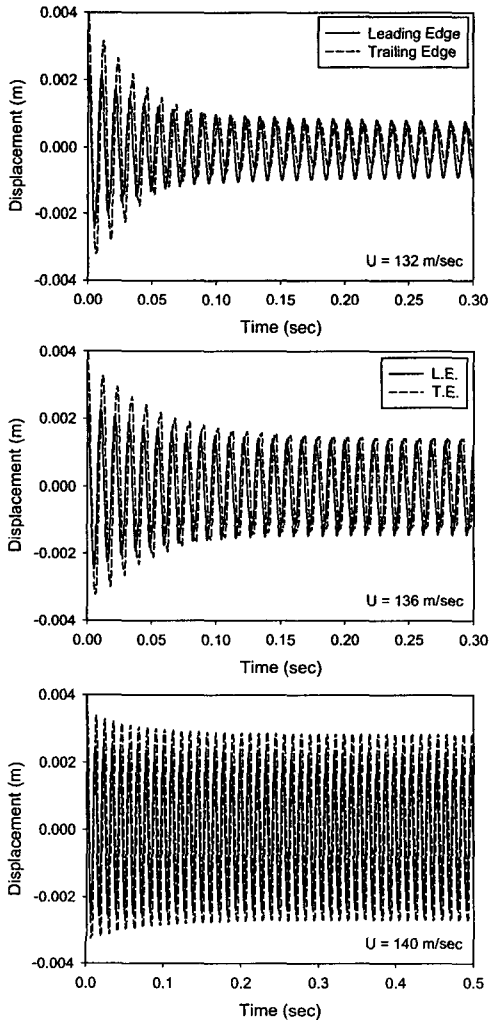

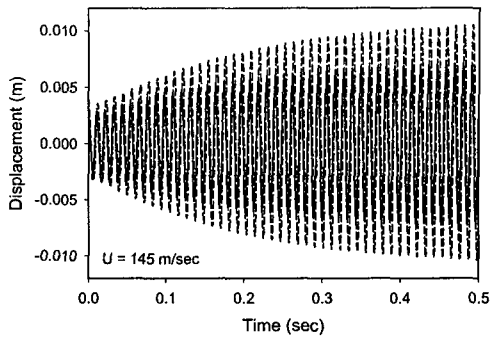

Fig. 6 Comparison of aeroelastic response for freeplay model (M=0.9, α_0=0 deg, s=0.2 deg, $q_1(0)$=0.0005).

Figure 7 shows the phase diagrams of nonlinear aeroelastic responses at Mach 0.9. At low velocity of 132 m/s, the phase diagram seems to be an elliptic type with weak nonlinearity. However, nonlinearity can be seen from higher velocities. One can also see the increment of oscillating amplitude according to an increased velocity. It is a typical trend of the nonlinear limit cycle oscillation due to flow-induced vibrations. Although not presented in this paper, the phase diagrams of the tip trailing edge (T.E) can be different from those of the tip leading edge (L.E). For the present model, large differences were observed at the cases of 136 and 140 m/s. It can be emphasized that a detrimental transonic flutter phenomenon may occur at very lower flight speed than that of predicted by ignoring the effect of freeplay.

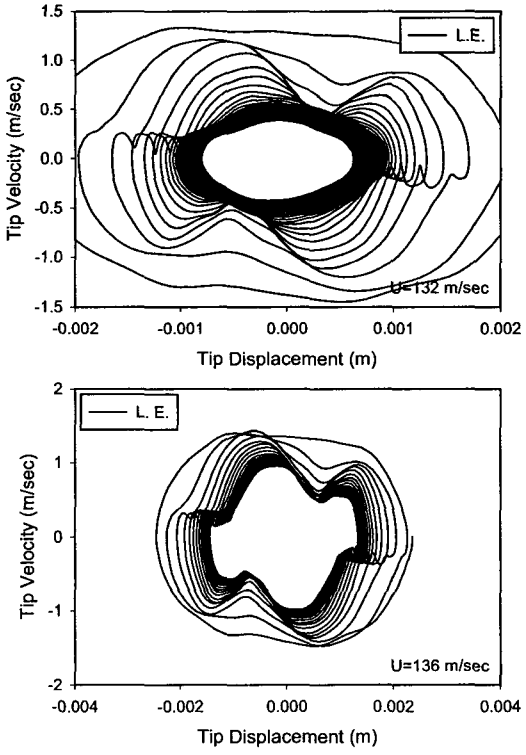

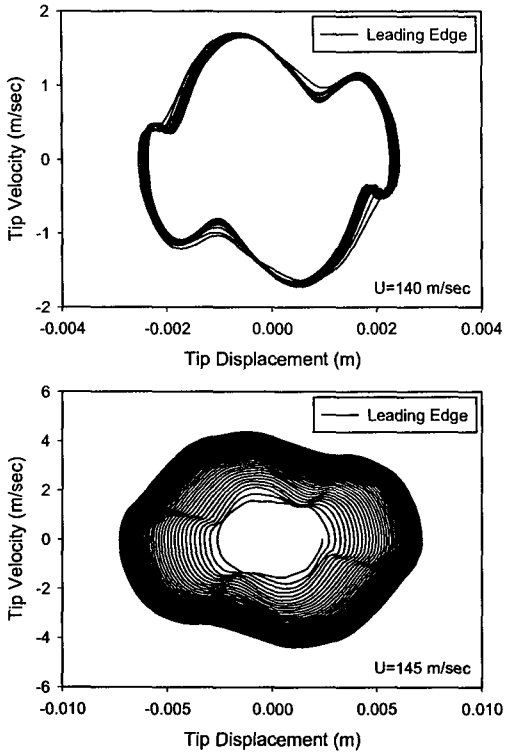

Fig. 7 Comparison of aeroelastic phase diagrams (M=0.9, α_0=0 deg, s=0.2 deg, $q_1(0)$=0.0005).

4. Concluding Remarks

In this study, a nonlinear aeroelastic analysis system has been developed using multidisciplinary numerical technologies. A generic missile control surface with all-movable pitch axis was considered to show the nonlinear characteristics of transonic aeroelasticity. One can see the successful and practical coupling of fictitious mass method (FMM) to typical coupled-time marching method (CTIM) using CFD. It is experienced from this study that the use of DMAP module of MSC/NASTRAN is needed to increase the numerical accuracy. Physically, it is found that a freeplay can introduce more unstable vibrations including limit cycle oscillations in the transonic flow region. This importantly indicates that a detrimental transonic flutter phenomenon can occur at very lower flight speed than that of predicted by ignoring the effect of freeplay. Thus, one has to pay attention to and carefully consider the unusual reduction effect of structural dynamic stability due to the freeplay nonlinearity. The developed computational system can be practically applied to the virtual flight test of aeroelastic instability for a canard wing and an all-movable stabilizer of high-speed generic fighters.

Acknowledgement

This work was supported by the Brain Korea 21 Project.

References

1. Laurenson, R. M., and Trn, R. M., "Flutter Analysis of Missile Control Surfaces Contating Structural Nonlinearities," *AIAA Journal*, Vol. 18, No. 10, October 1980, pp. 1245-1251.
2. Lee, C., "An Iterative Procedure for Nonlinear Flutter Analysis," *AIAA Journal*, Vol. 24, No. 5, May 1986, pp. 833-840.
3. Lee, B. H. K., and Torn, A., "Effect of Structural Nonlinearities of the CF-18 Aircraft," *Journal of Aircraft*, Vol. 26, No. 8, August 1989, pp. 781-786.
4. Lee, I. and Kim, S. H., "Aeroelastic Analysis of a Flexible Control Surface with Structural Nonlinearity," *Journal of Aircraft*, Vol. 32, No. 4, July-August 1995, pp. 868-874.
5. Karpel, M., Wieseman, C. D., "Modal Coordinates for Aeorelastic Analysis with Large Local Structural Variations," *Journal of Aircraft*, Vol. 31, No. 2, March-April 1994, pp. 396-400.
6. Karpel, M., Wieseman, C. D., "Time Simulation of Flutter with Large Stiffness Changes," *Journal of Aircraft*, Vol. 31, No. 2, March-April 1994, pp. 404-410.
7. Kim, D. H., Ji, S. G., Lee, I. and Kwon, J. H., "Transonic Aerodynamic Analysis Using Transonic Small Disturbance Equation," *Journal of The Korean Society for Aeronautical and Space Sciences*, Vol. 26, No. 2, April 1998, pp. 1-9.
8. Kim, D. H. and Lee, I., "Transonic and Low-Supersonic Aerodynamic Analysis of a Wing with Underpylon/Store," *Journal of Aircraft*, Vol. 37, No. 1, January-February 2000, pp. 189-192.
9. Kim, D. H. and Lee. I., "Transonic and Supersonic Flutter Characteristics of a Wing-Box Model with Tip Stores," 42nd AIAA/ASME/ASCE/AHS/ASC Structures, Structural Dynamics, and Materials Conf. & Exhibit Seattle, WC, 16-19 April 2001, AIAA Paper 2001-1464.
10. Kim, D. H. and Lee, I., "CFD-based matched-point transonic and supersonic flutter computations using a modified TSD equation," *Computational Fluid Dynamics Journal*, Vol. 11, No. 1, April 2002, pp. 35-49.
11. Kim, D. H., Park, Y. M. Lee, I. and Kwon O. J., "Nonlinear Aeroelastic Computation of a Wing with a Finned-Store Using a Parallel Unstructured Euler Solver", 43nd AIAA/ASME/ASCE/AHS/ ASC Structures, Structural Dynamics, and Materials Conf. & Exhibit, Denver, Colorado, 22-25 April 2002, AIAA Paper 1289.
12. Batina, J. T., "Efficient Algorithm for Solution of the Unsteady Transonic Small-Disturbance Equation," *Journal of Aircraft*, Vol. 25, No. 10, 1988, pp. 962-968.